Generalized self-consistent reservoir model for normal and anomalous heat transport in quantum harmonic chains

Kiminori Hattori and Miyuki Yoshikawa
Department of Systems Innovation, Graduate School of Engineering Science, Osaka University, Toyonaka, Osaka 560-8531, Japan

(Received 29 March 2019; published 4 June 2019)

Fictitious stochastic reservoirs incorporate scattering and dephasing mechanisms into the system in contact with these reservoirs. The reservoir-system coupling is described by the related self-energy in terms of the nonequilibrium Green's function formalism or equivalently the quantum Langevin equation formalism. In this study, we investigate thermal transport in a finite segment of an infinitely extended quantum harmonic chain with an equal self-energy at each site by using the self-consistent reservoir approach. In this setup, the entire system is lattice translation invariant so that mismatched boundaries are excluded from the model. Solving the Landauer-Büttiker equations under the self-consistent adiabatic condition, we quantitatively elucidate a thermally induced crossover of ballistic-to-diffusive transport and its scaling relation prescribed by a temperature-dependent mean free path. It is also shown that normal transport emerges in the diffusive limit for a linear self-energy, while nonlinear higher-order ones generically lead to anomalous transport. Physical implications of these observations are discussed in terms of the persistence of a massless Goldstone mode as well as the conservation of total linear momentum.

DOI: 10.1103/PhysRevE.99.062104

I. INTRODUCTION

Fourier's law of heat conduction is a phenomenological law that relates heat current to a temperature gradient as $\mathbf{J} = -\kappa\nabla\theta$, where κ is the material-dependent heat conductivity. For a small-enough temperature bias, this law predicts a linear temperature profile along the direction of heat flow in the steady state because of energy current continuity. It also follows that the heat current varies as $J \propto L^{-1}$, where L is the system size. In nonequilibrium statistical physics, it is a fundamental challenge to derive Fourier's law from first principles. This issue remains unresolved despite extensive theoretical studies thus far. From these studies, it is widely accepted at present that Fourier's law is genuinely broken in a low-dimensional lattice system without external forces that break total momentum conservation [1–5]. In particular, Fermi-Pasta-Ulam chains and disordered harmonic chains are the typical examples showing this anomaly. Heat transport that disobeys Fourier's law is termed as anomalous transport to distinguish it from normal transport that follows this law.

A linear harmonic chain coupled to a self-consistent reservoir (SCR) at each site is a simple model that reproduces normal transport. In the SCR model, thermal transport is analyzed self-consistently under the adiabatic condition that no net energy current flows into the inner reservoir. The fictitious stochastic reservoirs incorporate scattering and dephasing mechanisms into the system, analogously to Büttiker probes used to mimic inelastic scattering in electron transport [6–8]. The classical version of this model was first studied by Bolsterli *et al.* [9,10], and exactly solved by Bonetto *et al.* [11]. They showed a linear temperature profile and a finite thermal conductivity following Fourier's law in the thermodynamic limit. Recently, the classical model was extended to treat asymmetric harmonic chains [12,13] or anharmonic chains with on-site anharmonic potentials [14–16]. However, these models are valid only in the high temperature limit, since they assume the classical Langevin dynamics. The quantum version was first studied by Visscher and Rich [17] in terms of the quantum Langevin equation formalism. Subsequently, Dhar and Roy [18] derived the exact formula for a temperature dependent thermal conductivity in the thermodynamic limit. Roy [19] also investigated a crossover of ballistic and diffusive transport in finite-size systems by varying the coupling strength as well as the system size. The quantum model was recently used to investigate heat transport in harmonic chains with alternate masses [20] or spatial asymmetries [21,22].

Normally, the system where heat flux is induced is subjected to a temperature bias by connecting at both ends to external heat reservoirs sustained at different temperatures. The previous models mentioned above assume a finite chain linked to Ohmic reservoirs. In this situation, the system and the external reservoir have uncorrelated spectral properties so that interfacial scattering or temperature jumps ascribed to Kapitza resistance may occur at the boundaries between these two different substances [2–4]. These extrinsic factors tend to obscure the genuine bulk property of the system. It is also known that spectral properties of external reservoirs attached to the system may largely affect heat conduction even in the thermodynamic limit. Such a peculiarity is clearly exemplified in the study of mass disordered chains, where either vanishing or diverging thermal conductivity is observed, depending on the heat reservoirs present [23]. Thus, eliminating boundary mismatch is desirable for unambiguously capturing intrinsic features as well as for making theoretical analysis straightforward.

The reservoir-system coupling is described by the related self-energy in terms of the nonequilibrium Green's function formalism [24–26] or equivalently the quantum Langevin equation formalism [3,4,18]. In this study, we deal with an

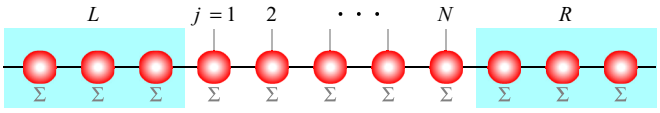

FIG. 1. An infinitely extended quantum harmonic chain with an equal self-energy Σ at each site. A central portion consisting of N lattice sites is regarded as the system, while two semi-infinite outer regions connecting to the system are viewed as leads, which are denoted as L and R. In the system, the self-energy is ascribed to an inner reservoir serving as a temperature probe, which is symbolized by a gray bar in this figure.

infinitely extended quantum harmonic chain with an equal self-energy at each site, for which problematic boundary mismatch is eliminated due to lattice translation invariance. We investigate thermal transport in a finite segment of this lattice by using the SCR approach. Solving the Landauer-Büttiker equations under the self-consistent adiabatic condition, we quantitatively elucidate a thermally induced crossover of ballistic-to-diffusive transport and its scaling relation prescribed by a temperature-dependent mean free path. We also generalize the self-energy function under the reality condition, including the ordinary Ohmic type adopted in the previous studies. This generalized SCR model accounts for normal and anomalous transport in a unifying manner and illuminates their relevance to the persistence of a massless Goldstone mode as well as the conservation of total linear momentum.

The paper is organized as follows. In Sec. II, we describe the Landauer-Büttiker formalism for our SCR model. The theoretical formulation is greatly simplified by virtue of translational symmetry. In Sec. III, we compare numerical results for two representative types of self-energies, leading to explicit physical insights into normal and anomalous transport. Finally, Sec. IV provides a summary.

II. THEORETICAL FORMULATION

We consider a quantum harmonic chain consisting of N lattice sites connected at both ends to two semi-infinite leads denoted as L (for left) and R (right), which act as external heat reservoirs. As shown in Fig. 1, at each site of the central system, we assume an equal on-site self-energy Σ ascribed to an inner reservoir, which serves as a temperature probe. Thus, we deal with heat transport in $N+2$ terminal system. To exclude boundary mismatch, the lead is taken to be a semi-infinite extension of the system, where the same self-energy Σ is incorporated at each site as that in the system. This is a generalization of the Rubin bath [3,4,23]. In this setup, the model describes a finite segment of an infinitely extended quantum harmonic chain with an equal self-energy at each site. In what follows, each terminal is labeled by $p \in \{1, 2, \ldots, N, L, R\}$, while the index notation $j \in \{1, 2, \ldots, N\}$ is used to denote a specific site contained in the system as well as a virtual probe attached to it.

A. Landauer-Büttiker formula and Green's function

We employ the Landauer-Büttiker formula for analyzing thermal transport, which is derived from the quantum Langevin equation formalism [3,4,18] as well as the nonequilibrium Green's function formalism [24–26]. In terms of the Landauer-Büttiker formula, heat current flowing in terminal p is described by $J_p = \sum_q G_{pq}(\theta_p - \theta_q)$ for a small-enough temperature difference $\theta_p - \theta_q$. The interterminal thermal conductance is expressed as $G_{pq} = h^{-1}\int_0^\infty d\varepsilon \frac{\partial f}{\partial \theta}\varepsilon T_{pq}$. Here $T_{pq} = \Gamma_p \Gamma_q |g_{pq}|^2$ is the transmission coefficient, g_{pq} is the retarded Green's function, Γ_p is the linewidth function, and $f = (e^{\varepsilon/k_B\theta} - 1)^{-1}$ is the Bose function for phonons. The thermal conductance quantum is defined by $G_0 = (\pi k_B)^2\theta/3h$ [27,28], which corresponds to G_{pq} for $T_{pq} = 1$. Note that in this notation, indices p and q are assigned to the sites connected to the relevant terminals for the correlation function g_{pq} of the system.

The retarded Green's function is analyzable in the recursive manner [4,25,29] formulated as $g_{NN} = ({g_0}^{-1} - s^4 g_{N-1,N-1})^{-1}$ and $g_{1N} = -s^2 g_{1,N-1} g_{NN}$, where $g_0 = (\varepsilon^2 - 2s^2 - \Sigma)^{-1}$ refers to the Green's function of an isolated site, $s = \hbar\sqrt{K/m}$ is the characteristic energy scale of the harmonic chain, K is the force constant, and m is the particle mass. For a semi-infinite chain, the surface Green's function obeys $g_{NN} = g_{N-1,N-1} \equiv g$. This leads to the quadratic Dyson equation $g = g_0(1 + s^4 g^2)$. The solution is found to be $g = -e^{-\alpha}/s^2$ and $\alpha = -2i \sin^{-1} z$, where $z = \mathrm{sgn}(\varepsilon)\sqrt{\varepsilon^2 - \Sigma}/2s$. As mentioned above, we consider a finite chain connected to two semi-infinite leads at both ends. In this configuration, the Green's functions are computed by adding sites one by one to an isolated lead until reaching the opposite lead. For a finite chain in contact with a semi-infinite lead, one easily finds $g_{11} = ({g_0}^{-1} - \overline{\Sigma})^{-1} = g$ and hence $g_{22} = \cdots = g_{NN} = g$, where $\overline{\Sigma} = s^4 g$ is the self-energy due to the lead. Note that g relates the two self-energies $\overline{\Sigma}$ and Σ. The Rubin model corresponds to $\overline{\Sigma}$ for $\Sigma = 0$. After coupling to the opposite lead, the end-site Green's function becomes $g_{NN} = -(2s^2 \sinh\alpha)^{-1}$. Analogously, the Green's function joining two ends is derived to be $g_{1N} = e^{-\alpha(N-1)} g_{NN}$. From these results, the internal Green's function is formulated as

$$g_{jj'} = -\frac{e^{-\alpha|j-j'|}}{2s^2 \sinh\alpha}, \tag{1}$$

since, generally, a two-point correlation function depends only on distance for a system with translational symmetry. It is easily shown that translational symmetry relates the real-space correlation function to the momentum-space correlation function via a Fourier transform

$$g_{jj'} = \frac{1}{2\pi}\int_{-\pi}^{\pi} dk \frac{e^{ik(j-j')}}{\varepsilon^2 - {\varepsilon_k}^2 - \Sigma},$$

where $\varepsilon_k = 2s|\sin(k/2)|$. In the previous study [18], Eq. (1) is deduced for an infinite chain from analytic matrix inversion. Following the formulation given above, the thermal conductance G_{pq} is also a function of distance between the associated sites such that $G_{jj'} = G_{|j-j'|}$, $G_{jL} = \overline{G}_{j-1}$ and $G_{jR} = \overline{G}_{N-j}$. The linewidth function Γ_p is given by $\Gamma = -2\,\mathrm{Im}\,\Sigma$ for probes and $\overline{\Gamma} = -2\,\mathrm{Im}\,\overline{\Sigma}$ for leads.

B. Consequences of lattice translation symmetry

Lattice translation invariance leads to additional constraints on the thermal conductance. Heat current flowing in

probe j is decomposed into

$$J_j = \sum_{j'} G_{jj'}(\theta_j - \theta_{j'}) + G_{jL}(\theta_j - \theta_L) + G_{jR}(\theta_j - \theta_R). \quad (2)$$

Suppose that the entire system stays at a temperature θ except a probe j where a temperature shift $\theta_j - \theta$ is induced. In this situation, Eq. (2) is reduced to $J_j = G_j(\theta_j - \theta)$, where $G_j = \Sigma_{j' \neq j} G_{jj'} + G_{jL} + G_{jR}$. Because of translational symmetry, G_j is position independent, i.e., $G_1 = G_2 = \cdots = G_N$. Moreover, two regions diverging from j can be viewed as semi-infinite leads. Thus, the problem we address is equivalent to a single site (i.e., $N = 1$) in contact with two leads maintained at the equal temperature θ. Then, it follows that $G_j = G_{1L} + G_{NR}$. Since $G_{1L} = G_{NR}$ due to inversion symmetry, we finally arrive at $G_j = 2G_{1L} = 2G_{NR}$.

To examine the temperature profile in a system linked to two leads held at unequal temperatures, it is convenient to define the dimensionless temperature $\Theta_j = (\theta_j - \theta)/\theta_{LR}$, where $\theta = (\theta_L + \theta_R)/2$ and $\theta_{LR} = \theta_L - \theta_R$. By definition, $\Theta_L = -\Theta_R = 1/2$ and $\Theta_{LR} = \Theta_L - \Theta_R = 1$. The self-consistent adiabatic condition $J_j = 0$ yields the N linear equations

$$\Theta_j = \sum_{j' \neq j} P_{jj'}\Theta_{j'} + P_{jL}\Theta_L + P_{jR}\Theta_R \quad (3)$$

for probe temperatures Θ_j at $j = 1, 2, \ldots, N$, where $P_{jj'} = G_{jj'}/G_j$, $P_{jL} = G_{jL}/G_j$, and $P_{jR} = G_{jR}/G_j$. The normalized conductance P obeys the sum rule

$$\sum_{j' \neq j} P_{jj'} + P_{jL} + P_{jR} = 1. \quad (4)$$

Furthermore, translational symmetry demands

$$P_{1L} = P_{NR} = 1/2. \quad (5)$$

The effective two-terminal conductance, expressed as

$$G = \frac{J_L}{\theta_{LR}} = G_{LR} - \sum_j G_{jL}(\Theta_j - \Theta_L), \quad (6)$$

correlates to Θ_j. An equivalent formulation is derived for J_R from the continuity of energy current in the steady state.

It may be instructive to show that probable temperature profiles can be intuitively deduced in the diffusive and ballistic limits without numerically solving Eq. (3). In the diffusive regime, it is reasonable to assume that the internal conductance like $G_{jj'}$ decays rapidly with distance and hence P is a short-ranged function. In this limit, one expects that $P_{jj'} = \frac{1}{2}\sum_{\pm}\delta_{j,j'\pm1}$, $P_{jL} = \frac{1}{2}\delta_{j,1}$ and $P_{jR} = \frac{1}{2}\delta_{j,N}$, where the factor $1/2$ stems from Eqs. (4) and (5). Interestingly, this assumption is equivalent to the Laplace equation $\frac{\partial^2}{\partial x^2}\Theta = 0$ or its lattice version $\Theta_j = (\Theta_{j+1} + \Theta_{j-1})/2$. It is easily seen that the lattice Laplace equation satisfying the boundary conditions $\Theta_0 = \Theta_L$ and $\Theta_{N+1} = \Theta_R$ is rearranged in the form of Eq. (3). The discretized equation is solved to be $\Theta_j = \frac{1}{2} - \frac{j}{N+1}$, which describes the linear temperature profile without discontinuities at the boundaries. On the other hand, P becomes a long-ranged function in the ballistic regime. Given Eqs. (4) and (5), one finds that $P_{jL} = P_{jR} = 1/2$ and thereby $P_{jj'} = 0$ in this limit. Then, the solution is $\Theta_j = (\Theta_L + \Theta_R)/2 = 0$, indicating that the internal temperature gradient vanishes and jumps in the temperatures at the boundaries are maximal.

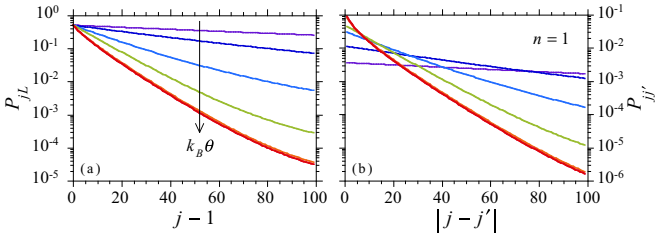

FIG. 2. Normalized conductance (a) P_{jL} and (b) $P_{jj'}$ as a function of intersite distance for $n = 1$. In the calculation, the coupling strength is taken as $\gamma/s = 0.1$, while the mean temperature is varied as $k_B\theta/s = 10^{-4}, 10^{-3}, 10^{-2}, \ldots, 10^{2}$.

III. NUMERICAL RESULTS AND DISCUSSION

In this section, we explore thermal transport in the present SCR model by using numerical calculations. The previous studies usually assume an Ohmic inner reservoir for which $\Sigma(\varepsilon) = -i\gamma\varepsilon$. This corresponds to a simple relaxation time approximation. In this study, we generalize the self-energy function into the form $\Sigma(\varepsilon) = -i\gamma\varepsilon^n$. The exponent n is restricted to odd integers, since $\Sigma(\varepsilon)$ should satisfy the reality condition $\Sigma(\varepsilon) = \Sigma^*(-\varepsilon)$. In the numerical calculations, $n = 3$ is chosen in addition to $n = 1$. It may be worth noting that

$$\Sigma(\varepsilon) = -\frac{i}{2s}\frac{\langle\delta m^2\rangle}{\langle m\rangle^2}\varepsilon^3$$

is derived for mass disordered harmonic chains to second order from perturbation theory, where $\langle m\rangle$ and $\langle\delta m^2\rangle$ denote the mean mass and the variance in mass, respectively [23,30,31]. This exemplifies that nonlinear self-energies are not unphysical.

A. Temperature profile and scaling relation

We begin by discussing probe temperatures for $n = 1$. Figure 2 shows the normalized conductance P as a function of intersite distance. As expected, P decays monotonically with the distance. It is also noticed that P_{1L} is invariable and fixed at $1/2$, as predicted by Eq. (5). A faster decay occurs as the mean temperature θ increases, implying that a thermally induced crossover from ballistic to diffusive transport is reproducible in this model. Figure 3 displays probe temperatures derived from numerically solving Eq. (3). As seen in the figure, the temperature profile is linear in the bulk with finite jumps at the boundaries. Recall that the present model is translationally invariant. Therefore, boundary mismatch is not the reason for the observed discontinuities. For a finite system of size N, the internal temperature difference $\Theta_{1N} = \Theta_1 - \Theta_N$ grows with increasing θ and then saturates to a finite value in the $\theta \to \infty$ limit. As $N \to \infty$, Θ_{1N} tends to approach unity over the entire range of θ. Note that the boundary jump is given by $(1 - \Theta_{1N})/2$.

The internal temperature gradient is quantitatively analyzable as follows. Assuming a linear profile such that $\Theta_j = R_N(\frac{1}{2} - \frac{j}{N+1})$, Eq. (3) leads to

$$\Theta_{1N} = \eta_N\left[\frac{R_N + 1}{2} - \frac{R_N(\xi_N + 1)}{N + 1}\right], \quad (7)$$

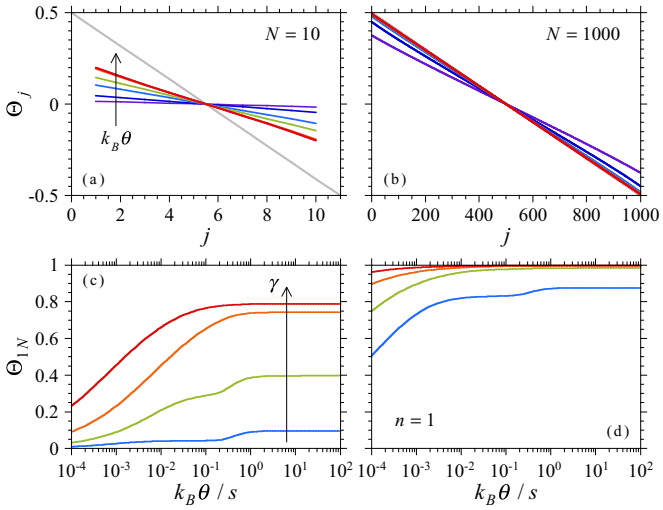

FIG. 3. Probed temperatures for $n = 1$. The upper panels show Θ_j for (a) $N = 10$ and (b) $N = 1000$. In the calculation, the coupling strength is taken as $\gamma/s = 0.1$, while the mean temperature is varied as $k_B\theta/s = 10^{-4}$, 10^{-3}, 10^{-2}, ..., 10^{2}. The gray line indicates the linear profile without boundary jumps as a reference. The lower panels display Θ_{1N} as a function of $k_B\theta$ for (c) $N = 10$ and (d) $N = 1000$. In the calculation, γ is varied as $\gamma/s = 10^{-2}$, 10^{-1}, 10^{0}, and 10^{1}.

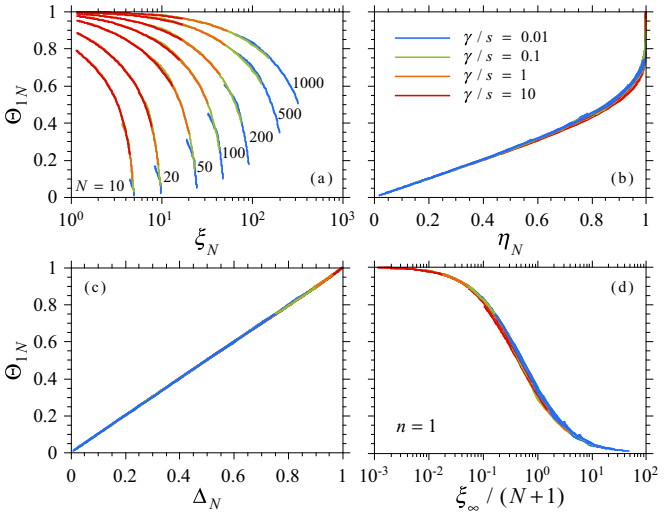

FIG. 4. Internal temperature difference Θ_{1N} scaled with (a) ξ_N, (b) η_N, (c) Δ_N and (d) $\xi_\infty/(N+1)$ for $n = 1$. In the calculation, the parameters are varied in the range $10 \leqslant N \leqslant 1000$, $10^{-2} \leqslant \gamma/s \leqslant 10$, and $10^{-4} \leqslant k_B\theta/s \leqslant 10^{2}$.

where

$$\eta_N = 2\sum_{j=2}^{N} P_{j1}, \tag{8}$$

$$\xi_N = \frac{\sum_{j=2}^{N} G_{j1}(j-1)}{\sum_{j=2}^{N} G_{j1}}. \tag{9}$$

In deriving these expressions, we exploited Eqs. (4) and (5), as well as $P_{jj'} = P_{|j-j'|}$. The factor R_N is eliminated by equating Eq. (7) to $\Theta_{1N} = R_N(1 - \frac{2}{N+1}) \equiv \Delta_N$. Consequently, we obtain

$$\Delta_N = \frac{\eta_N(1-\delta_N)}{(2-\eta_N)(1-\delta_N) + \eta_N\xi_N\delta_N}, \tag{10}$$

where $\delta_N = 2/(N+1)$. By definition, the reduced parameters η_N and ξ_N vary over the range $0 \leqslant \eta_N \leqslant 1$ and $1 \leqslant \xi_N \leqslant N/2$ for a finite system of size N. In the $N \to \infty$ limit, $P_{1R} = 0$ so that $\Sigma_{j=2}^{\infty} P_{j1} = 1/2$ in terms of Eqs. (4) and (5). This means $\eta_\infty = 1$. For an infinitely large system, the first moment of internal conductance $G_{jj'}$ is expressed as

$$\xi_\infty = \frac{\int_0^\infty d\varepsilon \frac{\partial f}{\partial\theta}\varepsilon \frac{\Gamma^2}{2|\sinh\alpha|^2\sinh^2\alpha_R}}{\int_0^\infty d\varepsilon \frac{\partial f}{\partial\theta}\varepsilon \frac{\Gamma^2\exp(-\alpha_R)}{|\sinh\alpha|^2\sinh\alpha_R}}, \tag{11}$$

where $\alpha_R = \mathrm{Re}\,\alpha$. From these results, a simple asymptotic form as $N \to \infty$

$$\Delta_N \sim \frac{1}{1 + 2\xi_\infty/(N+1)} \tag{12}$$

is obtained for a linear temperature profile. In view of Eq. (12), the effective mean free path [19] is evaluated to be $\ell = 2\xi_\infty$ in the thermodynamic limit.

The numerical data obtained over an extensive parameter range ($10 \leqslant N \leqslant 10^3$, $10^{-2} \leqslant \gamma/s \leqslant 10$ and $10^{-4} \leqslant k_B\theta/s \leqslant 10^2$) are summarized in Fig. 4 as a function of the reduced parameters given above. As seen in this figure, Θ_{1N} smoothly varies with η_N and ξ_N, and quantitatively agrees with Δ_N calculated from Eq. (10). Interestingly, all the data scaled with $\xi_\infty/(N+1)$ collapse onto a single curve and obey a scaling law $\Theta_{1N} = \mathcal{F}(\frac{\xi_\infty}{N+1})$. The scaling function is found to be $\mathcal{F}(x) = (1+2x)^{-1}$, which coincides with the right-hand side of Eq. (12) describing the asymptotic behavior. Thus, ballistic and diffusive regimes are simply classified by the effective length scale ξ_∞.

On the other hand, the result obtained for $n = 3$ is distinct from that for $n = 1$. In the case of $n = 3$, the temperature profile is nonlinear for a large θ in the vicinity of the boundaries, as shown in Fig. 5. This implies that heat transport becomes anomalous for nonlinear self-energies. Because of the anomaly, the above formulation assuming a linear profile is no longer validated rigorously. Nonetheless, Θ_{1N} does not largely deviate from Δ_N defined by Eq. (10), as shown in Fig. 6. It is also seen in this figure that a scaling behavior holds for asymptotically large N. The scaling function is found to be $\mathcal{F}(x) = (1+bx^{2/3})^{-3/2}$ with $b = 2^{2/3} - 1$. In view of this, the effective mean free path amounts to $\ell \simeq \xi_\infty$. [The data in the range $N \leqslant 50$ are not shown in Fig. 6(d). These data for small systems appreciably deviate from the scaling relation.]

Figure 7 compares ξ_∞ for $n = 1$ and $n = 3$. In both cases, ξ_∞ diminishes as temperature increases and approaches a certain finite value in the $\theta \to \infty$ limit. However, low temperature behaviors are quantitatively different; ξ_∞ varies as $\theta^{-1/2}$ for $n = 1$ and θ^{-2} for $n = 3$. The latter behavior accounts for a relatively rapid transition from (anomalous) diffusive to

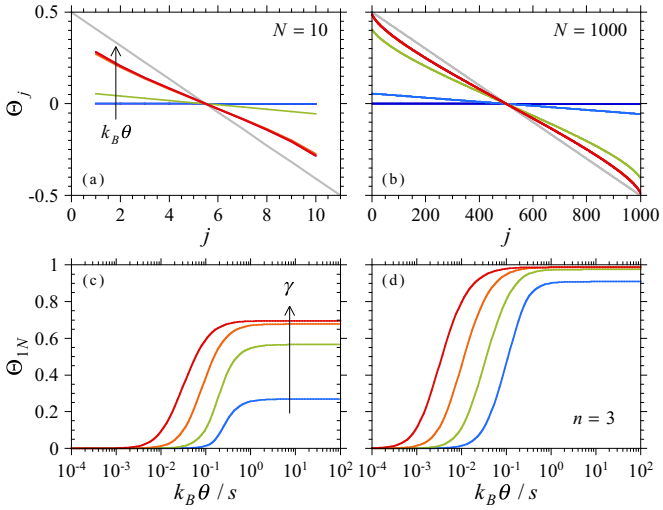

FIG. 5. Probed temperatures for $n = 3$. The upper panels show Θ_j for (a) $N = 10$ and (b) $N = 1000$. In the calculation, the coupling strength is taken as $\gamma s = 0.1$, while the mean temperature is varied as $k_B\theta/s = 10^{-4}, 10^{-3}, 10^{-2}, \ldots, 10^{2}$. The gray line indicates the linear profile without boundary jumps as a reference. The lower panels display Θ_{1N} as a function of $k_B\theta$ for (c) $N = 10$ and (d) $N = 1000$. In the calculation, γ is varied as $\gamma s = 10^{-2}$, 10^{-1}, 10^{0}, and 10^{1}.

ballistic regime with lowering θ (see, Fig. 5). The divergently enlarging ξ_∞ at low temperatures will be readdressed below.

It should be stressed here that the effective length scale ξ_∞ derived in the present study is explicitly temperature dependent. In contrast, the previous study using the SCR model for finite quantum chains [19] argues that the effective mean free path is unrelated to temperature. As shown in Fig. 7, this is valid only in a limited temperature range, particularly, the classical high-temperature regime.

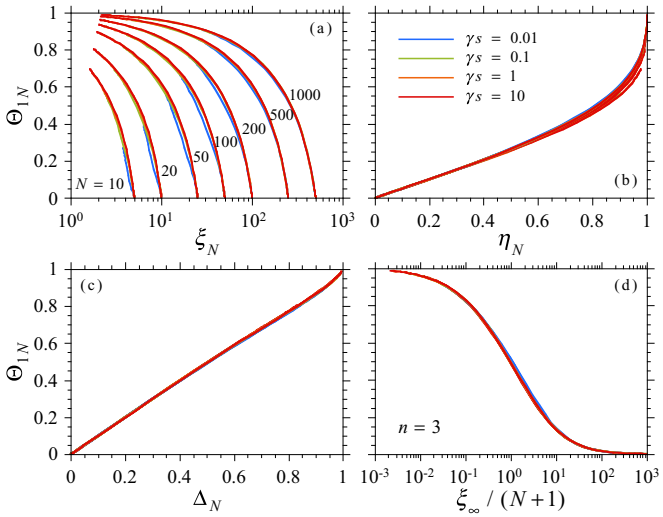

FIG. 6. Internal temperature difference Θ_{1N} scaled with (a) ξ_N, (b) η_N, (c) Δ_N and (d) $\xi_\infty/(N+1)$ for $n = 3$. In the calculation, the parameters are varied in the range $10 \leqslant N \leqslant 1000$, $10^{-2} \leqslant \gamma s \leqslant 10$ and $10^{-4} \leqslant k_B\theta/s \leqslant 10^{2}$. In (d), the data in the range $N \geqslant 100$ are chosen to show the asymptotic behavior.

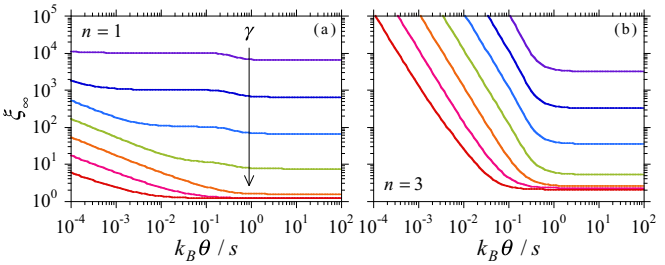

FIG. 7. Effective length scale ξ_∞ as a function of temperature $k_B\theta$ for (a) $n = 1$ and (b) $n = 3$. In the calculation, γ is varies as 10^{-4}, 10^{-3}, 10^{-2}, …, 10^{2} in units where $s = 1$.

B. Thermal conductivity and role of massless mode

Next, we address thermal conductivity. For a finite-sized system, the effective conductivity is usually defined as $\kappa_N = G(N+1)$ in accordance with Fourier's law. However, this expression is invalid when there exist temperature jumps at the boundaries. Regardless of the boundary jumps, the internal conductivity $\kappa_{1N} = G(N-1)/\Theta_{1N}$ may suitably describe heat conduction in the interior of the system. These two quantities coincide in the thermodynamic limit since $\Theta_{1N} \to 1$ as $N \to \infty$.

Prior to discussing numerical results, it may be appropriate to outline the analytic results derived in the thermodynamic limit [18]. The thermal conductivity is evaluated from internal bond currents in an infinite quantum chain to be

$$\kappa_\infty = \frac{1}{h}\int_0^\infty d\varepsilon \frac{\partial f}{\partial\theta}\varepsilon\mathcal{K}_\infty, \tag{13}$$

where

$$\mathcal{K}_\infty = -\frac{\Gamma\,\mathrm{Im}(\sinh\alpha)}{4s^2|\sinh\alpha|^2\sinh^2\alpha_R}. \tag{14}$$

To examine these expressions, it is important to note that $\lim_{\varepsilon\to 0}\frac{\varepsilon}{k_B}\frac{\partial f}{\partial\theta} = 1$. In the low energy limit $\varepsilon \to 0$, $\mathcal{K}_\infty$ behaves as $s/\sqrt{2\gamma\varepsilon}$ for $n = 1$ and $(2s/\gamma)\varepsilon^{1-n}$ for $n = 3, 5, 7, \ldots$. For the former, the integral $I = \int_0^d d\varepsilon\mathcal{K}_\infty$ is convergent for $0 < d < \infty$. This does not contradict a finite value of κ_∞ expected for $n = 1$. However, $I = \infty$ for the latter, and hence κ_∞ diverges for $n = 3, 5, 7, \cdots$ irrespective of temperature. Thus, the normal thermal conductivity is definable only for $n = 1$. For $n = 1$, κ_∞ increases with temperature until reaching the classical limit $\kappa_{\mathrm{cl}} = \pi k_B s^2/h\gamma$ [18].

The numerical results are displayed in Fig. 8. For $n = 1$, the effective conductivity κ_N increases with size N and tends to approach κ_∞ in the $N \to \infty$ limit. The internal conductivity κ_{1N} shows a similar tendency. However, quantitative aspects are different. In particular, κ_{1N} does not significantly deviate from κ_∞ even for a small N. This feature implies that Fourier-type transport is retained in the interior of the system. For $n = 3$, κ_N increases linearly with N at low temperatures, signaling ballistic transport. At high-enough temperatures, κ_N asymptotically varies as $\sqrt{N}$. The $\sqrt{N}$ dependence is also seen for κ_{1N} in the high temperature regime. The observed anomalous behavior agrees with the analytical and numerical results for mass disordered harmonic chains [3,4,30,32]. Regarding this observation, the following comment may be worth

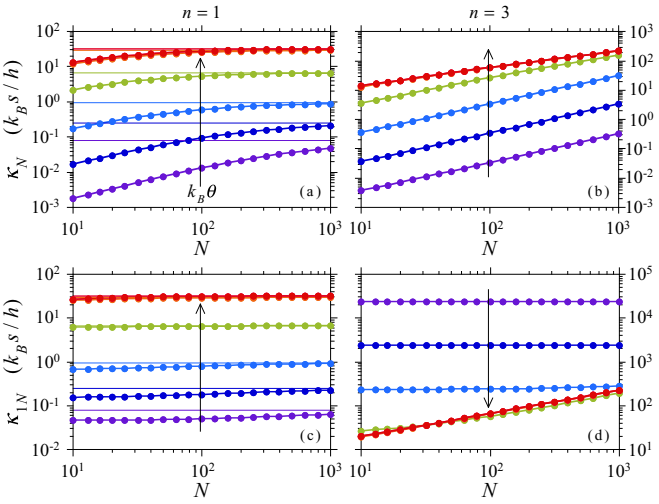

FIG. 8. Thermal conductivities [(a) and (b)] κ_N and [(c) and (d)] κ_{1N} as a function of system size N. The numerical results for $n = 1$ are shown in (a) and (c), while those for $n = 3$ in (b) and (d). In the calculation, γ is taken as 0.1 in units where $s = 1$, while $k_B\theta/s$ is varied as 10^{-4}, 10^{-3}, 10^{-2}, ..., 10^{2}. The thin horizontal line in (a) and (c) indicates κ_∞ for $n = 1$ as a reference.

mentioning. SCRs bring about not only phonon scattering but also phase breaking in the system coupled to these reservoirs. Clearly, phase decoherence is not caused by quenched disorder. Nevertheless, its essential features are reproduced by the SCR model of $n = 3$. The effect of dephasing on thermal transport, which cannot be decoupled in the present calculation, is an interesting subject of research in future. At low temperatures, κ_{1N} is almost independent of N for $n = 3$. This behavior is not indicative of normal transport. If θ is low enough, heat transport becomes ballistic in a finite-sized system so that $G \simeq G_0$, and concurrently $\Theta_{1N} \simeq 2(N+1)/\xi_\infty$ follows from the relevant scaling relation. As a result, $\kappa_{1N} \propto G_0\xi_\infty$ is apparently size independent. (Note that $G_0 \propto \theta$ and $\xi_\infty \propto \theta^{-2}$ result in $\kappa_{1N} \propto \theta^{-1}$.)

As demonstrated above, whether the anomaly in thermal transport disappears or emerges depends on the exponent n. To explore its physical implications, we finally examine the kinetics of the present model for all possible n. The displacement q_j of particle j from its equilibrium position obeys the equation of motion

$$m\left(\frac{\partial^2}{\partial t^2} + i^{n-1}\lambda\frac{\partial^n}{\partial t^n}\right)q_j + K(2q_j - q_{j+1} - q_{j-1}) = 0. \quad (15)$$

Here stochastic noise terms are neglected. The coupling strength is scaled as $\lambda = \hbar^{n-2}\gamma$. Note that q_j is a real number only for odd n. In terms of Eq. (15), the total linear momentum follows

$$\left(\frac{\partial}{\partial t} + i^{n-1}\lambda\frac{\partial^{n-1}}{\partial t^{n-1}}\right)\mathcal{P}(t) = 0. \quad (16)$$

For $n = 1$, the solution is $\mathcal{P}(t) = \mathcal{P}(0)e^{-\lambda t}$, indicating that total momentum conservation is broken. On the other hand, $\dot{\mathcal{P}}(t) = 0$ constitutes a physical solution and hence total momentum is conserved for $n = 3, 5, 7, \ldots$. Assuming a plane wave solution, Eq. (15) leads to the dispersion

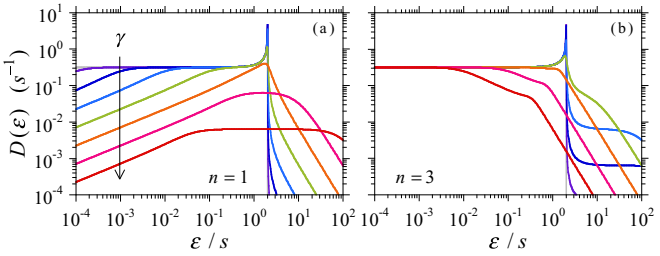

FIG. 9. Density of states $D(\varepsilon)$ for (a) $n = 1$ and (b) $n = 3$. In the calculation, γ is varied as 10^{-4}, 10^{-3}, 10^{-2}, ..., 10^{2} in units where $s = 1$. The gray line shows $D(\varepsilon)$ for $\gamma = 0$ as a reference.

equation $\omega^2 + i\lambda\omega^n - {\omega_k}^2 = 0$, where $\varepsilon_k = \hbar\omega_k$. In the long-wavelength limit $k \to 0$, the equation is solved to give $k = (\omega/c)\sqrt{1 + i\lambda\omega^{n-2}}$, where $c = s/\hbar$ is the phase velocity for $\lambda = 0$. In the low-frequency limit $\omega \to 0$, the solution is reduced to $k = \sqrt{i\lambda\omega}/c$ for $n = 1$ and $k = \omega/c$ for $n = 3, 5, 7, \ldots$. This indicates that the propagating mode with no excitation gap no longer exists for $n = 1$, whereas it remains intact for $n = 3, 5, 7, \ldots$. It is reasonable to consider that the persistent massless mode correlates with a divergently large mean free path and the resulting ballistic transport at low temperatures. The massless mode also relates to the density of states, which is given by $D(\varepsilon) = -(2\varepsilon/\pi)\,\mathrm{Im}\,g_{jj}(\varepsilon)$ per site [29]. In the low energy limit $\varepsilon \to 0$, $D(\varepsilon)$ is expressed as $(\pi s)^{-1}\sqrt{\varepsilon/2\gamma}$ for $n = 1$ and $(\pi s)^{-1}$ for $n = 3, 5, 7, \ldots$. These analytical results are confirmed in Fig. 9, where the numerical results are shown for various γ. The vanishing massless mode predicted for $n = 1$ is reflected in $D(\varepsilon)$, which vanishes in the $\varepsilon \to 0$ limit. This is in contrast to a low energy plateau exhibited by $D(\varepsilon)$ for $n = 3$.

These observations imply that thermal transport becomes normal in the diffusive limit when total momentum conservation is violated and the massless mode vanishes, whereas anomalous transport occurs as long as total momentum is conserved and the massless mode persists. The present conclusion derived for quantum-mechanical chains in an extended parameter range reinforces the prevailing conjecture deduced in the classical limit [1–5].

Before ending this section, we give an additional support to the above conclusion. The massless mode can be eliminated by adding an arbitrary small but finite linear self-energy to the cubic one, since the former is the leading term at sufficiently low energies. As expected, Fourier's law followed by a finite thermal conductivity is then recovered in the thermodynamic limit.

IV. SUMMARY

We have investigated thermal transport in a finite segment of an infinitely extended quantum harmonic chain with an equal self-energy at each site by using the SCR approach. In this setup, mismatched boundaries are excluded from the model due to lattice translation invariance. Solving the Landauer-Büttiker equations under the self-consistent adiabatic condition, we quantitatively elucidate a thermally induced crossover of ballistic-to-diffusive transport and its scaling relation prescribed by a temperature dependent mean

free path. We generalize the self-energy function under the reality condition. It is shown that normal transport emerges in the diffusive limit for a linear self-energy, while nonlinear higher-order ones generically lead to anomalous transport. In the former case, total momentum conservation is violated and a massless Goldstone mode vanishes, whereas in the latter case, total momentum is conserved and the massless mode persists. These observations for quantum-mechanical chains reinforce the prevailing conjecture deduced in the classical limit.

ACKNOWLEDGMENTS

This work was supported by a Grant-in-Aid for Scientific Research (Grant No. 18K03977) from the Japan Society for the Promotion of Science.

[1] F. Bonetto, J. L. Lebowitz, and L. Rey-Bellet, in *Mathematical Physics 2000*, edited by A. Fokas, A. Grigoryan, T. Kibble, and B. Zegarlinski (Imperial College Press, London, 2000), pp. 128–150.
[2] S. Lepri, R. Livi, and A. Politi, Phys. Rep. **377**, 1 (2003).
[3] A. Dhar, Adv. Phys. **57**, 457 (2008).
[4] S. Lepri (Ed.), *Thermal Transport in Low Dimensions* (Springer, Heidelberg, 2016).
[5] T. Prosen and D. K. Campbell, Phys. Rev. Lett. **84**, 2857 (2000).
[6] M. Büttiker, Phys. Rev. B **33**, 3020 (1986).
[7] S. Datta, *Electronic Transport in Mesoscopic Systems* (Cambridge University Press, Cambridge, 1995).
[8] Y. Imry, *Introduction to Mesoscopic Physics* (Oxford University Press, New York, 2008).
[9] M. Bolsterli, M. Rich, and W. M. Visscher, Phys. Rev. A **1**, 1086 (1970).
[10] M. Rich and W. M. Visscher, Phys. Rev. B **11**, 2164 (1975).
[11] F. Bonetto, J. L. Lebowitz, and J. Lukkarinen, J. Stat. Phys. **116**, 783 (2004).
[12] E. Pereira and H. C. F. Lemos, Phys. Rev. E **78**, 031108 (2008).
[13] D. Segal, Phys. Rev. E **79**, 012103 (2009).
[14] E. Pereira and R. Falcao, Phys. Rev. E **70**, 046105 (2004).
[15] E. Pereira, Phys. Rev. E **82**, 040101(R) (2010).
[16] E. Pereira, R. Falcao, and H. C. F. Lemos, Phys. Rev. E **87**, 032158 (2013).
[17] W. M. Visscher and M. Rich, Phys. Rev. A **12**, 675 (1975).
[18] A. Dhar and D. Roy, J. Stat. Phys. **125**, 801 (2006).
[19] D. Roy, Phys. Rev. E **77**, 062102 (2008).
[20] A. F. Neto, H. C. F. Lemos, and E. Pereira, Phys. Rev. E **76**, 031116 (2007).
[21] M. Bandyopadhyay and D. Segal, Phys. Rev. E **84**, 011151 (2011).
[22] E. Pereira, Phys. Lett. A **374**, 1933 (2010).
[23] A. Dhar, Phys. Rev. Lett. **86**, 5882 (2001).
[24] T. Yamamoto and K. Watanabe, Phys. Rev. Lett. **96**, 255503 (2006).
[25] J.-S. Wang, J. Wang, and J. T. Lü, Eur. Phys. J. B **62**, 381 (2008).
[26] S. G. Das and A. Dhar, Eur. Phys. J. B **85**, 372 (2012).
[27] L. G. C. Rego and G. Kirczenow, Phys. Rev. Lett. **81**, 232 (1998).
[28] K. Schwab, E. A. Henriksen, J. M. Worlock, and M. L. Roukes, Nature (London) **404**, 974 (2000).
[29] K. Hattori and Y. Nakamura, Phys. Rev. B **97**, 224312 (2018).
[30] H. Matsuda and K. Ishii, Prog. Theor. Phys. Suppl. **45**, 56 (1970).
[31] A. J. O'Connor and J. L. Lebowitz, J. Math. Phys. **15**, 692 (1974).
[32] R. J. Rubin and W. L. Greer, J. Math. Phys. **12**, 1686 (1971).